# Measurement of Adhesion Force To Determine Surface Composition in an Electrochemical Environment

**Joseph M. Serafin and Andrew A. Gewirth***

*Department of Chemistry and Frederick Seitz Materials Research Laboratory, University of Illinois at Urbana−Champaign, Urbana, Illinois 61801*

*Received: July 17, 1997*[⊗]

Adhesion force measurements are used to determine potential dependence of the force of adhesion between a $Si_3N_4$ cantilever and an Au surface in basic solution. At both positive and negative potentials, the force curve is dominated by van der Waals contributions, indicating that there is little specific interaction between the tip and the sample. However, at intermediate potentials (between 0.4 and 0.6 V vs SHE) the tip−sample interaction is dominated by an adhesive component, the magnitude of which is approximately 2 kJ/mol; this corresponds to the expected strength of a hydrogen bond between $O^-$ groups on the tip and AuOH on the surface.

## Introduction

The composition and structure of an electrode surface determines its catalytic and electrochemical properties. Consequently, one of the main objectives of electrochemistry is the elucidation of the structure as well as the potential dependence of that structure. Adsorption on electrodes is of particular importance, as the redox states of the adsorbates on electrode surfaces profoundly affect the electronic and chemical properties.

Methods to determine the in situ structure of the adsorbate lattice include X-ray reflectivity[1] and atomic force and scanning tunneling microscopies (AFM and STM, respectively).[2] Knowledge of the composition of adsorbates on electrodes is a crucial field of inquiry as their nature and identity profoundly affect electrode properties in areas as diverse as catalysis,[5e] deposition,[2] and corrosion.[6] For example, in the area of underpotential deposition, the importance of coadsorption of anions to surface structural and catalytic properties has been demonstrated,[2,7] and knowledge of the chemical composition of the coadsorbates continues to be of great value in interpreting structural studies. Methods developed to determine surface composition include chronocoulometry,[3] quartz crystal microbalance (QCM),[4] and various interface-sensitive optical spectroscopies.[5]

In this paper, we use adhesion measurements to monitor the adsorption and eventual oxidation of an adsorbate on an initially clean electrode surface. Specifically, the formation of a monolayer of $OH^-$ on Au(111) and the further oxidation of AuOH to gold oxide, AuO, are examined.

The use of the AFM for adhesion measurements has received considerable attention recently[8−23] and is sometimes referred to as chemical force microscopy (CFM). One of the main advantages of using an AFM, as compared to the surface force apparatus (SFA)[24] or interfacial force microscope (IFM),[25] is that the AFM probe can afford a high degree of spatial resolution. Indeed, specific chemical interactions have been used for imaging in frictional force microscopy.[26]

In the AFM-based adhesion measurements performed to date, a wealth of useful chemical information has been obtained, including measurements down to single interactions being performed.[10,11] In a typical experiment, both the probe and sample surface are covered with a functionalized self-assembled monolayer (SAM), and the surface−surface interaction is determined. In this manner, quantities such as the surface and interfacial free energy[24] can be determined. The adhesion measurements can serve as sensitive probes of the variations in the chemical interactions and surface energies and have been extended to pH titration[16,23,26b] or oxidation-state dependence.[18,20,22,26c]

A related experimental methodology[27−42] is the examination of the tip−surface approach force curves to determine the surface charge in the framework of DLVO theory.[43] In this manner, many important values such as the isoelectric point, or point of zero charge, can be determined. In the electrochemical environment, Arai and Fujihira[41] used the approaching tip−sample force profiles to determine that specific adsorption of anions had occurred.

The focus of this paper is on adhesion force measurements as a probe of electrochemical events, in particular, the specific chemical interaction between a probe and the bare or adsorbate-modified electrode surface. Two similar experimental approaches have been adopted by Hudson et al.[18] and Marti[26c] where adhesion or friction is used to monitor potential-dependent changes on the electrode. Hudson et al.[18] coated the probe and sample surface with a conducting polymer and found the adhesion to depend on the oxidation state of the polymer. This can be quite useful for imaging, as the hydrophilic and hydrophobic regions have different adhesion values with either oxidation state of the polymer, allowing for the possibility of chemical contrast frictional imaging without changing tips, which introduces complications that can make comparisons problematic. The experiments of Marti[26c] investigate the frictional properties of an electrode surface under potential control, and evidence of chemical specificity was observed. In an experiment by Green et al.,[22] the oxidation state of a surface bound redox species was monitored by examining the change in the adhesion in a potential dependence manner.

Results presented by Raiteri et al.,[20] who examined the potential dependence of the variation in the adhesive force of a $Si_3N_4$ probe surface on a gold electrode in various electrolyte solutions, are closely related to results presented here. In their experiment, the potential-dependent variations in the adhesion could not be explained except for the somewhat trivial case where the adhesion was reduced from an increase in the double-layer repulsion. The adhesion force variations could not be correlated with voltammetric features and hence could not be

[⊗] Abstract published in *Advance ACS Abstracts,* November 15, 1997.

S1089-5647(97)02338-9 CCC: $14.00 © 1997 American Chemical Society

explained. As will be discussed below, a possible explanation for their adhesion force results for the gold oxidation potential region will be presented that would bring their results into agreement with the presented results.

One of the most significant advantages, and limitations, of adhesion-based measurements is that they can be highly surface specific. This condition provides for a method of direct determination of the surface and, as such, can provide a direct measurement of properties that would otherwise have to be indirectly measured. In this paper, the formation of an oxide monolayer on Au(111) in basic solution is examined. In acidic solution, it is known that oxygen is buried under gold atoms in the potential region where AuO forms.[44] The process whereby the Au and O exchange places is sometimes referred to as "turnover". Voltammetric data[45] suggested that the turnover occurs after the formation of AuOH in acid, but subsequent experiments[44] determined that turnover did not occur until the formation of gold oxide. STM imaging studies[44] that use surface roughening to infer turnover have demonstrated that surface roughening does not occur until AuO formation under acidic conditions. However, there have not been STM images of this nature from Au surfaces under basic conditions. Adhesion measurements, such as the one presented in this paper, can provide a direct measurement of the surface composition. The measurements reported in this paper provide direct evidence as to the state of the electrode surface under basic conditions.

## Experimental Section

The Au sample substrates were prepared by annealing Au-coated glass (Dirk Schröer, Berlin) in a $H_2$ flame just prior to use (see ref 7). The surface crystallinity was confirmed using the imaging mode of the AFM; this also allowed for the precise positioning of the probe surface to the center of a large atomically flat crystallite. All solutions were prepared with ultrapure water (Millipore Q) and sodium hydroxide monohydrate (Suprapure grade, EM Science). Potential control was maintained with a CV-27 potentiostat (Bioanalytical Systems) using a three-electrode configuration. The counter and pseudoreference electrodes were both flame-annealed Au wires. Absolute voltage calibration was achieved by comparison of voltammetry in the sample cell with voltammetry obtained using a $Hg/HgSO_4$ reference electrode. All solutions were deoxygenated prior to use, and the adhesion force measurements were performed under a slight positive pressure of $N_2$. All potentials reported are relative to NHE.

The adhesion measurements were performed in a commercial AFM apparatus (Molecular Imaging), using commercial control and data acquisition electronics (Nanoscope III, Digital Instruments). The AFM adhesion measuring apparatus is shown in Figure 1. In this arrangement, the electrode is fixed in space and the probe surface is scanned. The working electrode is clamped in place with the Teflon cell that contains the supporting electrolyte solution. The probe surface and supporting V-shaped cantilever are mechanically coupled to the *X, Y, Z* piezoelectric crystal with the glass rod assembly. The cantilever deflection is monitored using the optical lever arm method. The laser beam is transmitted through the glass rod to the tip of the cantilever and reflected back along the glass rod to the position-sensitive detector (PSD).

The probe surface was a commercial $Si_3N_4$ AFM tip. The surface of the $Si_3N_4$ is predominately covered by $Si-O^-$ groups under the experimental conditions (pH = 11−12).[16] The deflection sensitivity of the instrument was calibrated against the linear response in the region of constant compliance, and the scanning piezoelectric crystal was calibrated by imaging a grating of known dimensions. V-shaped cantilevers were used for these experiments, as the spring constants of the torsional modes are large for this geometry.[14] The variation in the spring constant between AFM wafers is notoriously high, and it is thus necessary to calibrate the spring constant of the cantilevers. Fortunately, the variation in the spring constant across a wafer is quite small and can be quite satisfactorily obtained from averaging a few sample cantilevers on a given wafer.[14,46] The force constants of the cantilevers were estimated from the resonance frequency of the cantilever and the manufacturer's specifications of the length and width of the cantilever legs.[46] All of the cantilevers used in this study were gold-coated to increase the reflectivity of the probe diode beam. Without the reflective gold coating, the optical interference from the gold electrode resulted in a large oscillatory background signal at the PSD which hindered discrimination of the cantilever deflection. The effect of the gold reflective coating was accounted for in the calculation of the force constant.[47] We estimate the error in the force constant based on the length and width dimensions and the resonance frequency to be not more than a factor of 2.

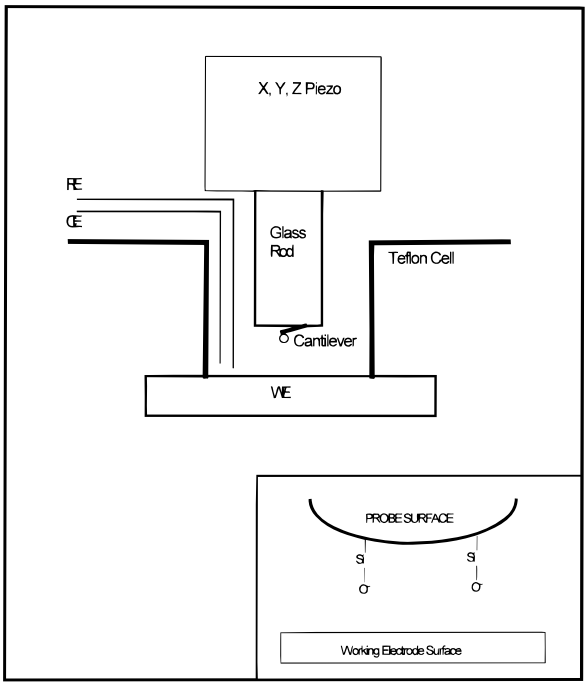


**Figure 1.** Schematic of experimental arrangement. In this arrangement, the working electrode, WE, is Au(111) and is fixed in space. The counter and reference electrodes, CE and RE, are both gold wires. The cantilever that holds the $Si_3N_4$ probe surface is attached to the glass rod assembly; the glass rod is connected to the *X, Y, Z* piezoelectric scanner. The electrolyte solution is housed in the Teflon cell. Shown in the insert is a simplified representation of the $Si_3N_4$ probe surface.

## Results

Shown in Figure 2 is a cyclic voltammogram of Au(111) oxidation in 0.01 M NaOH. There are three distinct potential regions of interest in the voltammetry.[48] Potential region I corresponds to the potential region where no adsorption of OH or O is known to occur. The first oxidative feature, "A", corresponds to the specific adsorption of $OH^-$ on Au(111).[48] Potential region II is the potential region where AuOH is known to be present on the surface and begins at $OH^-$ adsorption, "A", and extends to the second oxidative feature, "B", which corresponds to the further oxidation of AuOH to AuO.[48] Potential region III corresponds to the presence of gold oxide at or near the surface and begins with the formation of oxide, "B".

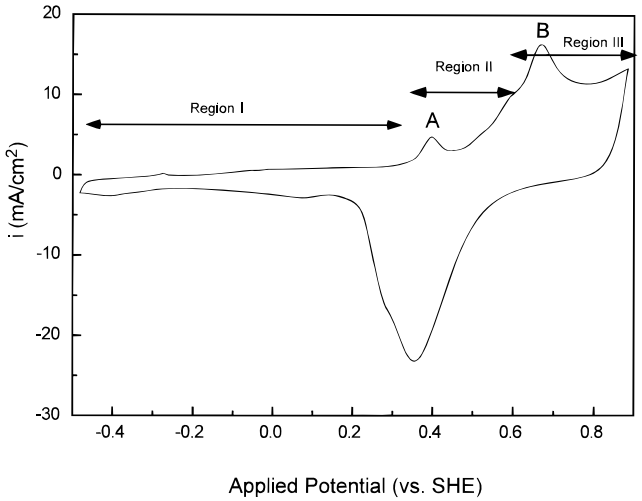


**Figure 2.** Cyclic voltammetry of 0.01 M NaOH on Au (111). The scan rate was 50 mV/s. The oxidation feature, "A", at 0.4 V corresponds to the specific adsorption of OH−. The second oxidative feature, "B", corresponds to the formation of gold oxide. Scanning the potential from negative to positive potentials, the voltammetry can be divided into three potential regions. Potential region I corresponds to bare gold, potential region II corresponds to the presence of AuOH, and potential region III corresponds to the presence of gold oxide.

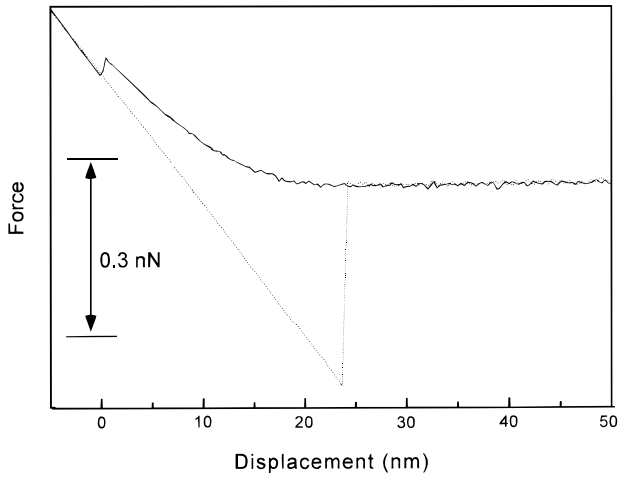


**Figure 3.** Representative tip−sample approach and retraction force curve at 210 mV on Au(111) in 0.01 M NaOH. Shown in the solid line is the tip−surface approach curve with a characteristic double-layer repulsion. Shown in the dashed line is the tip−sample retraction force curve. Reported adhesion forces are determined from the difference between the retraction curve minimum and the force at large separation.

The adhesion force is obtained from the force vs cantilever displacement profiles. Shown in Figure 3 is a sample graph of a typical force measurement taken at ∼200 mV, in potential region I, bare gold. The solid line in Figure 3 is the tip−surface approach, with a characteristic double-layer repulsion[24] which is evidenced by the roughly exponential displacement of the cantilever on approach. The dashed line is the tip−surface retraction, where the $Si_3N_4$ surface is pulled off of the electrode once the restoring force of the cantilever exceeds the adhesion force on the $Si_3N_4$ probe surface. For all force profiles presented, the zero separation distance is taken as the onset of constant compliance.

Between the potential regions I, II, and III, a marked variation in the adhesive force was observed. Shown in Figure 4 are three sample adhesion graphs from potential regions I, II, and III. The adhesion in region II, where AuOH is present,[48] is much larger than either region I, bare gold, or region III, gold oxide. Comparisons of the adhesion between regions I, bare gold, and III, gold oxide, are complicated by experimental scatter and will not be addressed.

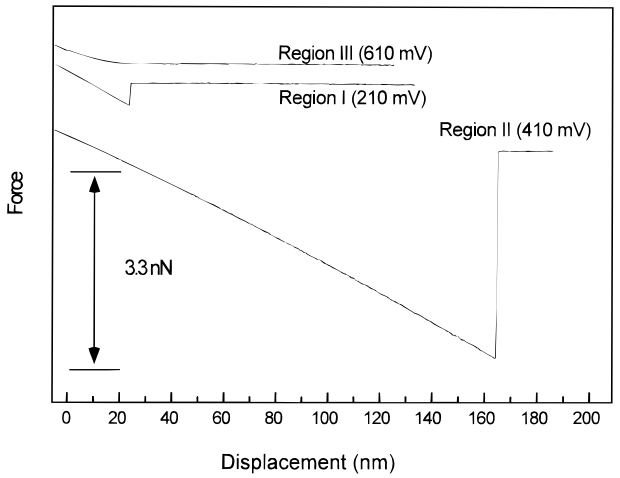


**Figure 4.** Representative adhesion force vs pull out displacement curves for potential regions I, II, and III. The zero of displacement corresponds to the onset of constant compliance for the tip−surface approach curves.

## Discussion

**A. Work of Adhesion.** The adhesion force, $F_{ad}$, between a probe and sample surface can be related to the work of adhesion, $W_{ad}$. The following discussion will use JKR theory,[49] as JKR theory has demonstrated success in a wide variety of applications. It should be noted that DMT[50] theory has also met with considerable success; however, as the discrepancy between the works of adhesion as derived from the adhesion force between the two approaches is only ∼30%, the experimental error of the presented data precludes quantitative comparison.

In JKR theory, $F_{ad}$ and $W_{ad}$ are related as

$$F_{ad} = -^3/_2 \pi R_T W_{ad} \quad (1)$$

where $R_T$ is the radius of curvature of the probe surface. The radius of curvature of the commercial $Si_3N_4$ tips have manufacturer's specifications of 5−20 nm.[51] However, in a series of experiments, the radius of curvature, $R_T$, was observed to vary considerably under the present experimental conditions, even when all the $Si_3N_4$ tips were from the same wafer. Whether this is a result of dispersion of the radii of curvature in the manufactured tips or a result of the experimental conditions (i.e., fracture, particle accumulation, etc.) is not known.

**B. Determination of Radius of Curvature.** It is desirable to have an in situ method for determination of the radius of curvature of the probe surface. An approach recently developed uses long-range double-layer forces to determine the radius of curvature of the probe surface.[36] However, this approach may not be appropriate for small distances. We adopt a methodology similar to that proposed by Hutter and Bechhoefer,[52] where the shorter range van der Waals force is used for the calibration. A nonretarded Hamaker constant, $A_H$, of $13 \times 10^{-20}$ J is estimated[24] from an average geometric mean of the $Si_3N_4$/water/$Si_3N_4$ $A_H$ value of $(5-6) \times 10^{-20}$ J[53] and $A_H$ of $(25-40) \times 10^{-20}$ J for gold/water/gold.[54] The van der Waals interaction energy between a sphere and a surface is described in the nonretarded limit[55] as

$$W_{vdw}(d) = -A_H R_T / 6d \quad (2)$$

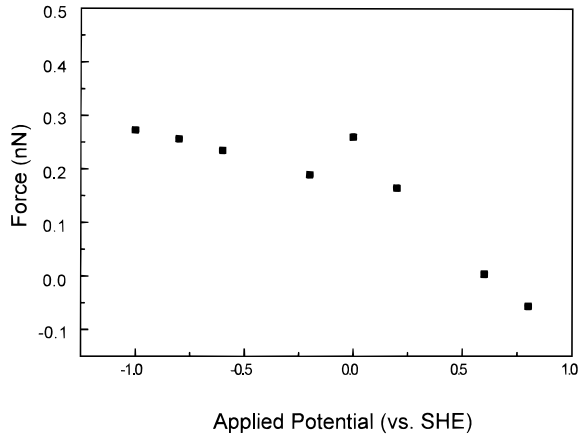


**Figure 5.** Graph of the force associated with double-layer repulsion measured 3 nm off of the surface as a function of applied potential obtained in a 1 mM NaOH solution from Au(111).

where $d$ is the sphere−surface distance; eq 2 is valid for the case where $d \ll R_T$. The force on the sphere is

$$F_{vdw}(d) = -A_H R_T/3d^2 \quad (3)$$

For the passive cantilevers used in AFM force measurements, there exists a region of mechanical instability when the force gradient of the potential exceeds the spring constant of the cantilever,[42] $k_s$,

$$\partial F/\partial d = k_s \quad (4)$$

At this instability, the probe surface will jump into contact with the surface with a characteristic "snap-in" distance, $d_s$, which is obtained from combining eqs 3 and 4,

$$d_s = (A_H R_T/3k_s)^{1/3} \quad (5)$$

Thus, the radius of curvature, $R_T$, is determined over a short-range measurement, namely $d_s$. Although the snap-in distance, $d_s$, can be measured even in the presence of double-layer forces, it is nontrivial to separate the double-layer and van der Waals forces at the short distances of 1−4 nm. Indeed, a further complication is the possibility of structural forces at these distances which cause deviations from DLVO-type descriptions.[24] It is desirable to measure the snap-in distance, $d_s$, in the absence of double-layer repulsion. A convenient approach in this study was to use dilute solutions (≤1 mM) of NaOH, where the $Si_3N_4$ surface charge is greatly reduced. Shown in Figure 5 is a graph of the double-layer repulsion measured 3 nm off of the surface. As can be seen in Figure 5, there exists a potential region where the double-layer repulsion goes to zero, at ∼0.6 V. It should be noted that this potential region corresponds to region III, AuO formation; however, comparisons in a different electrolyte, $CuSO_4/H_2SO_4$, where the $Si_3N_4$ tip is uncharged, showed only a small difference in the snap-in distance between the potential regions before and after AuO formation.

Shown in Figure 6 are sample tip−surface approach curves at 0.6 V, in 1 mM NaOH. No double-layer repulsion is observed. Owing to the relatively sparse density of points, from the digitization in the commercial software, it is difficult to determine the snap-in distance from a single measurement. However, from multiple measurements, the snap-in distance, $d_s$, can be determined to 2 ± 0.2 nm. It should be noted that this measurement can only provide an upper limit to the snap-in distance as oscillations about the equilibrium value will cause the mechanical instability to be sampled at larger equilibrium

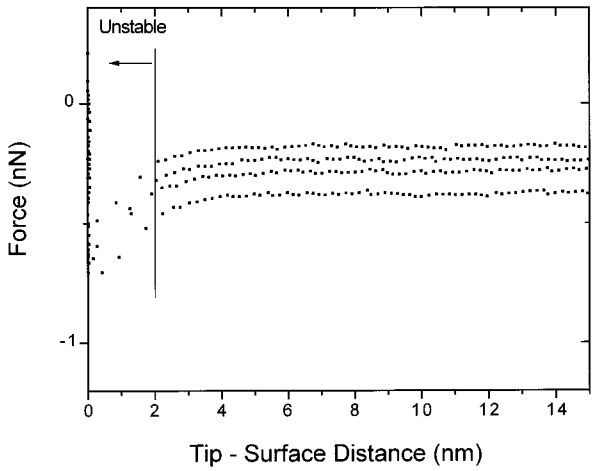


**Figure 6.** Tip−surface approach force profile. The probe surface is $Si_3N_4$, and the electrode surface is gold oxide. From these force profiles a region of mechanical instability is observed; the force gradient exceeds the spring constant of the cantilever.

distances. Rearranging eq 5 yields

$$R_T = 3k_s d_s^3/A_H \quad (6)$$

The inferred radius of curvature, $R_T$, is 35 nm.

**C. Potential Dependence of Work of Adhesion.** Once $R_T$ is known, the work of adhesion, $W_{ad}$, can be divided[56] as

$$W_{ad} = W_{vdw} + W_{se} + W_{hb} \quad (7)$$

where $W_{vdw}$ is the work of adhesion due to the van der Waals interaction and other electrostatic interactions, $W_{se}$ is the work done in solvent exclusion,[19] and $W_{hb}$ is the work done in hydrogen bonding. The work of adhesion can also be divided[19] as

$$W_{ad} = g_{Si_3N_4/H_2O} + g_{gold/H_2O} - g_{int} \quad (8)$$

where $g_{Si_3N_4/H_2O}$ is the surface free energy of the $Si_3N_4$ in water, $g_{gold/H_2O}$ is the surface free energy of gold in water, and $g_{int}$ is the interfacial free energy. In potential regions I and III, the Au(111) crystallite surface is composed of gold atoms, and as such the $W_{hb}$ term should go to zero in those potential windows. More specifically,

$$W_{ad}(I,III) = W_{vdw} + W_{se} \quad (9)$$

However, in potential region II, the $W_{hb}$ does not go to zero; indeed it dominates the interaction,

$$W_{ad}(II) = W_{vdw} + W_{se} + W_{hb} \quad (10)$$

If one assumes that the solvent exclusion and van der Waals interactions are approximately the same in all three regions, combining eqs 9 and 10 yields

$$W_{ad}(II) - W_{ad}(I,III) = W_{hb} \quad (11)$$

The above assumption is not unreasonable, as the adhesion forces, $F_{ad}(I,III)$, in potential regions I and III are quite comparable and much less than the adhesion force, $F_{ad}(II)$, in potential region II. The data presented in Figure 7 were obtained using the same probe surface calibrated above, $R_T$ = 35 nm; also shown in Figure 7 with solid circles is the double-layer repulsion force measured 3 nm off of the electrode surface. Shown in the open circles is the measured adhesion force, $F_{ad}$, at sample pull off. The adhesion force is clearly much larger

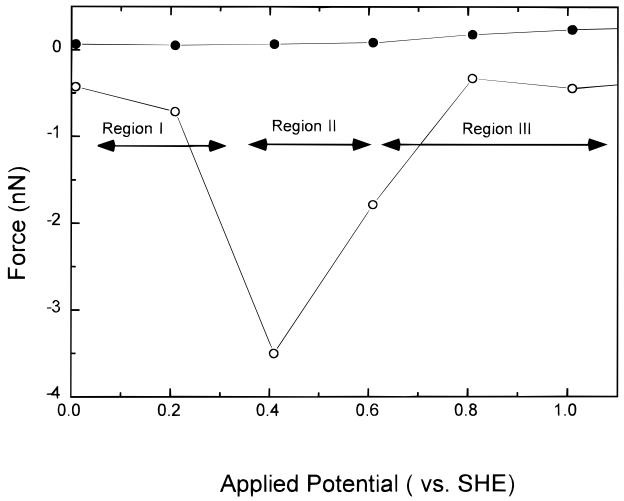


**Figure 7.** Shown in the solid circles is the double-layer repulsion 3 nm off of the onset of constant compliance for a $Si_3N_4$ probe surface with the Au(111) surface in 10 mM NaOH. The open circles are the adhesion force determined at liftoff.

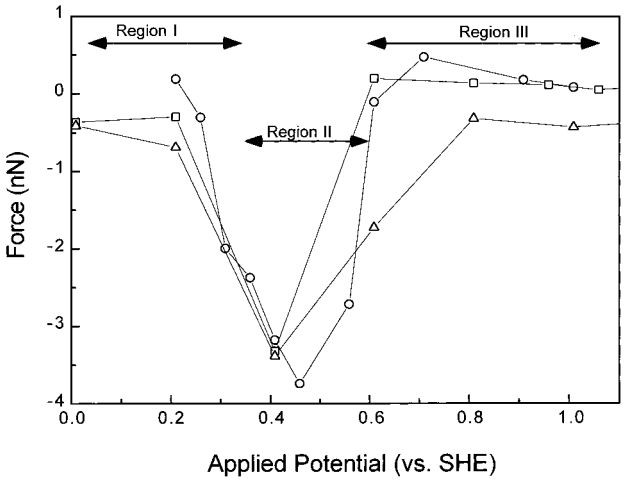


**Figure 8.** Plot of adhesion force vs applied potential for gold oxidation on Au(111) in 0.01 M NaOH with a $Si_3N_4$ probe surface. Each data set represents a different cantilever, tip, and Au(111) crystallite.

than the double-layer force in potential region II. Using an average measured adhesion force, $F_{ad}$(I,III), and eq 1, a work of adhesion of 2 mJ/m$^2$ is obtained. The maximum adhesion force in potential region II, $F_{ad}$(II), yielded a work of adhesion of 22 mJ/m$^2$. Using eq 11, a $W_{hb}$ value of 20 mJ/m$^2$ is obtained. Using a Si−O$^-$ surface density, the predominant surface functional group under these experimental conditions,[16] of five groups/nm$^2$,[10] a bond energy of 2 kJ/mol or 0.6 kcal/mol is obtained. Shown in Figure 8 are the results of three independent adhesion measurements with different AFM tips and cantilevers on different electrode surfaces; qualitatively similar results were obtained with 1 mM NaOH solution.

We note that the assumption that $W_{se}$ is the same in all three potential regions may not be reasonable as water likely hydrogen bonds with the AuOH surface in region II but not with the AuO or Au materials. However, the interaction of water with the cantilever is approximately the same in all three potential regions. If $W_{se}$ is not constant across the three regions and especially if it is larger in potential region II, then the value of $W_{hb}$ we report here will likely be too high. Accounting for changes in $W_{se}$ would require changing the solvent which is problematic because electrochemical formation of AuOH and AuO is poorly characterized in solvents other than water.

**D. Comparison with Other Results.** It remains to be determined what types of bonding interaction are occurring between the probe and electrode surface in potential region II. Thomas et al.[25] determined the hydrogen bond energy from the work of adhesion for two −$NH_2$-terminating SAM surfaces to be 1.3 kcal/mol in $N_2$. A value of 5 kcal/mol was obtained for two −COOH-terminated surfaces in $N_2$.[25] Owing to the similarity of these bond energies, the increased adhesion force in potential region II is determined to be due to hydrogen bonding between the groups on the probe surface with the gold surface; as −OH is the only specifically adsorbed entity, the interaction must be with AuOH. This is conclusive evidence that AuOH does not "turn over",[48] i.e., that the OH functionality remains on the electrode surface—in basic solution. In this regard, the behavior of Au in acidic and basic solutions is very similar. Finally, it should be noted that the Si−O$^-$ surface density and AuOH surface density[48] are rather different, and the lack of registry may lead to a reduced force of adhesion.

The total work of adhesion for potential region II, $W_{ad}$(II), compares well with the values of 54 and 17 mJ/m$^2$ for an acid−base adhesion AFM study[14] of an acid and base SAM in pure water and 0.3 M NaCl, respectively; however, the role of hydrogen exchange in this system is not clear. It also compares well with the two −COOH SAM functionalized surface adhesion force measurement of 16 mJ/m$^2$ in water,[19] as well as the two −$CONH_2$ functionalized SAM surface work of adhesion of 19 mJ/m$^2$ in water.[19] However, comparisons of this nature are nontrivial as all the factors in eq 7 must be separated for comparison. It appears that the interaction between the probe surface and the electrode surface in potential region II, AuOH present, is comparable to systems where hydrogen bonding is known to occur, and we thus propose that as the adhesion mechanism in potential region II.

The adsorption of −OH anions on the gold surface in the study of Raiteri et al.[20] offers a possible explanation of the adhesion results obtained. In particular, the observation that adhesion increases before gold oxide formation and then decreases at gold oxide formation is consistent with interaction of their probe surface with AuOH. Also, the lack of correlation between voltammetric features and adhesive force is explained with the observation that Cl$^-$ is known to suppress the −OH adsorption wave[57] in voltammetry.

## Conclusion

We offer this paper as proof of principle that adhesion-based measurements can be used to monitor adsorption at electrode surfaces and the subsequent oxidation of adsorbates. With suitable choice of tip chemistry, available through functionalized polystyrene spheres, determination of the chemical identity and coverage of other adsorbates should be possible, and this is work in progress.

**Acknowledgment.** This work was funded by Department of Energy Grant DE-FG02-91ER45349 through the Materials Research Laboratory at the University of Illinois.

## References and Notes

(1) (a) Toney, M. F.; Melroy, O. R. In *Electrochemical Interfaces: Modern Techniques for In-Situ Interface Characterization*; Abruna, H. D., Ed.; VCH: Berlin, 1991; p 57. (b) Toney, M. F.; Gordon, J. G.; Melroy, O. R. *SPIE Proc.* **1991**, *140*, 1550. (c) Toney, M. F. In *Synchrotron Techniques in Interfacial Electrochemistry*; Melendies, C. A., Tadjeddine, A., Eds.; Kluwer: Dordrecht, 1994. (d) Ocko, B. M.; Wang, J. In *Synchrotron Techniques in Interfacial Electrochemistry*; Melendies, C. A., Tadjeddine, A., Eds.; Kluwer: Dordrecht, 1994; p 109.

(2) Gewirth, A. A.; Niece, B. K. *Chem. Rev.* **1997**, *97*, 1129.

(3) (a) Shi, Z.; Lipkowski, J. *J. Electroanal. Chem*. **1995**, *365*, 1994. (b) Shi, Z.; Lipkowski, J. *J. Electroanal. Chem*. **1995**, *364*, 289. (c) Shi, Z.

C.; Lipkowski, J. *J. Phys. Chem.* **1995**, *99*, 4170. (d) Savich, W.; Sun, S. G.; Lipkowski, J.; Wieckowski, A. *J. Electroanal. Chem.* **1995**, *388*, 233. (e) Niece, B. K.; Gewirth, A. A. *Langmuir* **1996**, *12*, 4909.

(4) (a) Buttry, D. A.; Ward, M. D. *Chem. Rev.* **1992**, *92*, 1355. (b) Bruckenstein, S.; Hillman, R. A. In *The Handbook of Surface Imaging and Visualization*; Hubbard, A. T., Ed.; CRC Press: Boca Raton, FL, 1994; p 101.

(5) (a) Benziger, J. In *The Handbook of Surface Imaging and Visualization*; Hubbard, A. T., Ed.; CRC Press: Boca Raton, FL, 1994; p 265. (b) Corn, R. M.; Higgins, D. A. In *The Handbook of Surface Imaging and Visualization*; Hubbard, A. T., Ed.; CRC Press: Boca Raton, FL, 1994; p 479. (c) Pemberton, J. E. In *The Handbook of Surface Imaging and Visualization*; Hubbard, A. T., Ed.; CRC Press: Boca Raton, FL, 1994; p 647. (d) Hall, R. B. In *The Handbook of Surface Imaging and Visualization*; Hubbard, A. T., Ed.; CRC Press: Boca Raton, FL, 1994; p 755. (e) Weaver, M. J. *J. Phys. Chem.* **1996**, *100*, 13079.

(6) Lomakina, S. V.; Shatova, T. S.; Kazansky, C. P. *Corros. Sci*. **1994**, *36*, 1645.

(7) Will, T.; Dietterle, M.; Kolb, D. M. In *Nanoscale Probes of the Solid/Liquid Interface*; Gewirth, A. A., Siegenthaler, H., Eds.; NATO ASI Series, Series E, Vol. 288; Klumer Academic Publishers: Boston, 1995; p 137.

(8) Burnham, N. A.; Dominguez, D. D.; Mowery, R. L.; Colton, R. J. *Phys. Rev. Lett.* **1990**, *64*, 1931.

(9) Weisenhorn, A. L.; Maivald, P.; Butt, H.-J.; Hansma, P. K. *Phys. Rev. B* **1992**, *45*, 11226.

(10) Hoh, J. H.; Cleveland, J. P.; Prater, C. B.; Revel, J.-P.; Hansma, P. K. *J. Am. Chem. Soc.* **1992**, *114*, 4917.

(11) Lee, G. U.; Kidwell, D. A.; Colton, R. J. *Langmuir* **1994**, *10*, 354.

(12) Biggs, S. *Langmuir* **1995**, *11*, 156.

(13) Han, T.; Williams, J. M.; Beebe, Jr., T. P. *Anal. Chim. Acta* **1995**, *307*, 365.

(14) Noy, A.; Frisbie, C. D.; Rozsnyai, L. F.; Wrighton, M. S.; Lieber, C. M. *J. Am. Chem. Soc.* **1995**, *117*, 7943.

(15) Berger, C. E. H.; van der Werf, K. O.; Kooyman, R. P. H.; de Grooth, B. G.; Greve, J. *Langmuir* **1995**, *11*, 4188.

(16) Senden, T. J.; Drummond, C. J. *Colloids Surf. A*: *Physiochem. Eng. Aspects* **1995**, *94*, 29.

(17) Carpick, R. W.; Agrait, N.; Ogletree, D. F.; Salmeron, M. *Langmuir* **1996**, *12*, 3334.

(18) Hudson, J. E.; Abruna, H. D. *J. Am. Chem. Soc.* **1996**, *118*, 6303.

(19) Sinniah, S. K.; Steel, A. B.; Miller, C. J.; Reutt-Robey, J. E. *J. Am. Chem. Soc.* **1996**, *118*, 8925.

(20) Raiteri, R.; Grattarola, M.; Butt, H.-J. *J. Phys. Chem.* **1996**, *100*, 16701.

(21) Eastman, T.; Zhu, D.-M. *Langmuir* **1996**, *12*, 2859.

(22) Green, J.-B. D.; McDermott, M. T.; Porter, M. D. *J. Phys. Chem.* **1996**, *100*, 13342.

(23) Vezenov, D. V.; Noy, A.; Rozsnyai, L. F.; Lieber, C. M. *J. Am. Chem. Soc.* **1997**, *119*, 2006.

(24) Israelachvili, J. *Intermolecular and Surface Forces*, 2nd ed.; Academic Press: San Diego, 1994.

(25) Thomas, R. C.; Houston, J. E.; Crooks, R. M.; Kim, T.; Michalske, T. A. *J. Am. Chem. Soc.* **1995**, *117*, 38.

(26) (a) Green, J.-B. D.; McDermott, M. T.; Porter, M. D.; Siperko, L. M. *J. Phys. Chem.* **1995**, *99*, 10960 and references therein. (b) Marti, A.; Hahner, G.; Spencer, N. D. *Langmuir* **1995**, *11*, 4632 and references therein. (c) Weilandt, E.; Menck, A.; Binggeli, M.; Marti, O. In *Nanoscale Probes of the Solid/Liquid Interface*; Gewirth, A. A., Siegenthaler, H., Eds.; NATO ASI Series, Series E, Vol. 288; Klumer Academic Publishers: Boston, 1995; p 307 and references therein.

(27) Butt, H.-J. *Biophys. J.* **1991**, *60*, 1438.

(28) Ducker, W. A.; Senden, T. J.; Pashley, R. M. *Nature* **1991**, *353*, 239.

(29) Ducker, W. A.; Senden, T. J.; Pashley, R. M. *Langmuir* **1992**, *8*, 1831.

(30) Li, Y. Q.; Tao, N. J.; Pan, J.; Garcia, A. A.; Lindsay, S. M. *Langmuir* **1993**, *9*, 637.

(31) Larson, I.; Drummond, C. J.; Chan, D. Y. C.; Grieser, F. *J. Am. Chem. Soc.* **1993**, *115*, 11885.

(32) Lin, X.-Y.; Creuzet, F.; Arribart, H. *J. Phys. Chem.* **1993**, *97*, 7272.

(33) Kekicheff, P.; Marcelja, S.; Senden, T. J.; Shubin, V. E. *J. Chem. Phys.* **1993**, *99*, 6098.

(34) Biggs, S.; Mulvaney, P.; Zukoski, C. F.; Grieser, F. *J. Am. Chem. Soc.* **1994**, *116*, 9150.

(35) Ishino, T.; Hieda, H.; Tanaka, K.; Gemma, N. *Jpn. J. Appl. Phys.* **1994**, *33*, L1552.

(36) Drummond, C. J.; Senden, T. J. *Colloids Surf. A*: *Physiochem. Eng. Aspects* **1994**, *87*, 217.

(37) Arai, T.; Fujihira, M. *J. Electroanal. Chem.* **1994**, *374*, 269.

(38) Biggs, S.; Mulvaney, P. *J. Chem. Phys.* **1994**, *100*, 8501.

(39) Larson, I.; Drummond, C. J.; Chan, D. Y.; Grieser, F. *J. Phys. Chem.* **1995**, *99*, 2114.

(40) Hieda, H.; Ishino, T.; Tanaka, K.; Gemma, N. *Jpn. J. Appl. Phys.* **1995**, *34*, 595.

(41) Arai, T.; Fujihira, M. *J. Vac. Sci. Technol. B* **1996**, *14*, 1378.

(42) Hillier, A. C.; Kim, S.; Bard, A. J. *J. Phys. Chem.* **1996**, *100*, 18808.

(43) (a) Derjaguin, B. V.; Landau, L. *Acta Physiochim. URSS* **1941**, *14*, 633. (b) Verway, E. J. W.; Overbeek, J. Th. G. *Theory of Stability of Lyophobic Colloids*; Elsevier: Amsterdam, 1948.

(44) Vitus, C. M.; Davenport, A. J. *J. Electrochem. Soc.* **1994**, *141*, 1291 and references therein.

(45) (a) Angerstein-Kozlowska, H.; Conway, B. E.; Hamelin, A.; Stoicoviciu, L. *Electrochim. Acta* **1986**, *31*, 1051. (b) Angerstein-Kozlowska, H.; Conway, B. E.; Hamelin, A.; Stoicoviciu, L. *J. Electronal. Chem.* **1987**, *228*, 429.

(46) Cleveland, J. P.; Manne, S.; Bocek, D.; Hansma, P. K. *Rev. Sci. Instrum.* **1993**, *64*, 403.

(47) Sader, J. E.; Larson, I.; Mulvaney, P.; White, L. R. *Rev. Sci. Instrum.* **1995**, *66*, 3789.

(48) (a) Strbac, S.; Hamelin, A.; Adzic, A. A. *J. Electroanal. Chem.* **1993**, *362*, 47 references therein. (b) Hamelin, A. *J. Electroanal. Chem.* **1996**, *407*, 1.

(49) Johnson, K. C.; Kendall, K.; Roberts, A. D. *Proc. R. Soc. London, Ser. A* **1971**, *324*, 301.

(50) Derjaguin, B. V.; Muller, V. M.; Toporov, Y. P. *J. Colloid Interface Sci.* **1975**, *53*, 314.

(51) NP−S, oxide sharpened $Si_3N_4$ tips, Digital Instruments, Santa Barbara.

(52) Hutter, J. L.; Bechhoefer, J. *Rev. Sci. Instrum.* **1993**, *64*, 1868.

(53) Ackler, H. D.; French, R. H.; Chiang, Y. M. *J. Colloid Interface Sci.* **1996**, *179*, 460.

(54) (a) Schrader, M. E. *J. Colloid Interface Sci.* **1984**, *100*, 372. (b) Rabinovich, Ya. I.; Churaev, N. V. *Russ. J. Phys. Chem.* **1990**, *52*, 256.

(55) Derjaguin, B. V. *Kolloid Z.* **1934**, *69*, 155.

(56) Fowkes, F. M. *J. Phys. Chem.* **1962**, *66*, 682.

(57) Cahan, B. D.; Villullas, H. M.; Yeager, E. B. *J. Electroanal. Chem.* **1991**, *306*, 213.